

## Properties of the UCHII region G25.4NW and its associated molecular cloud \*

Mei Ai, Ming Zhu, Li Xiao and Hong-Quan Su

National Astronomical Observatories, Chinese Academy of Sciences, Beijing 100012, China;  
[xl@nao.cas.cn](mailto:xl@nao.cas.cn)

Received 2012 November 14; accepted 2013 April 12

**Abstract** Ultra compact HII (UCHII) G25.4NW is a bright IR source in the region of the inner Galaxy. New HI images from the Very Large Array Galactic Plane Survey show clear absorption features associated with the UCHII region up to  $95 \text{ km s}^{-1}$ , and there are no other absorptions up to the tangential velocity. This reveals that G25.4NW has a near-side distance of 5.7 kpc, and it is located in the region of the inner Galactic molecular ring. Using the new distance, the bolometric luminosity of G25.4NW is estimated as  $10^{5.6} L_{\odot}$ , which corresponds to an O6 star. It contains  $460 M_{\odot}$  of ionized gas. A high-resolution  $^{13}\text{CO}$  image from the Galactic Ring Survey reveals that G25.4NW is part of a more extended star-forming complex with about  $10^4 M_{\odot}$  of molecular gas.

**Key words:** radiation mechanisms: thermal — ISM: atoms — ISM: HII regions — ISM: molecules

### 1 INTRODUCTION

Formation of massive stars plays an important role in galaxy evolution. Ultra compact HII (UCHII) regions are indicators of sites where high mass stars form. In these regions, newly born stars are still embedded in their natal molecular clouds. The energy from the central massive stars is absorbed by the ambient dust and reradiated in the infrared (IR), making UCHII regions among the brightest IR sources in the Galaxy.

G25.4NW is a UCHII region, first identified by Lester et al. (1985), which is found to have the highest FIR luminosity in the region of the inner spiral arm, hosted in the giant molecular cloud (GMC) G25.4–0.14. It is also on the list of the top two sources of IR-luminosity among the 18 radio-selected UCHII regions studied by Gieveon et al. (2007). Recently, a massive protostar ( $6\text{--}12 M_{\odot}$ ) was found in the massive SCUBA core JCMT18354–0649S (Zhu et al. 2011), which is about  $1'$  south of G25.4NW. It is believed to lie in the same molecular cloud as G25.4NW based on the smooth change of  $^{13}\text{CO}$  and  $^{18}\text{CO}$  spectral profiles. Spectral line studies of JCMT18354–0649S show that both infall and outflow motions are seen in the envelope of gas that surrounds this source (Wu et al. 2005; Liu et al. 2011; Carolan et al. 2009), suggesting that this source is actively

---

\* Supported by the National Natural Science Foundation of China.

accumulating material and thus can potentially grow to an even more massive object as it evolves. It is a middle mass object, and might be in an early state that is a precursor of the UCHII region. Hence G25.4NW and the region near JCMT18354–0649S represent one of the most active star forming sites in the inner spiral arm.

However, there has been considerable uncertainty about the distance to the UCHII region G25.4NW. Downes et al. (1980) and Turner (1979) assigned a far-side distance of 13.5 kpc to G25.4NW based on absorption features in the H<sub>2</sub>CO and OH lines at  $\sim 96 \text{ km s}^{-1}$ , which was thought to be close to the tangent point velocity. Solomon et al. (1987) suggested a far-side distance of 11.5 kpc, based on the scale height of the molecular cloud. The papers by Lester et al. (1985) and Churchwell et al. (1990) used the far-side distance of 9.8 kpc for the UCHII region G25.4NW and they estimated a far-IR luminosity of  $L_{\text{FIR}} = 10^{6.238} L_{\odot}$ , indicating the presence of an O4 or O5 star. However, Givon et al. (2007) found that the mid-IR spectral type of G25.4NW was consistent with a B1 or an O9-O7 star (based on the mid-IR dust temperature, with an  $L_{\text{MIR}} = 10^{4.3} - 10^{5.2} L_{\odot}$ ). This suggests that the stars are not as hot as indicated by the far-IR data.

In the case of JCMT18354–0649S, Zhu et al. (2011) also found that if the far-side distance of 9.6 kpc was used, the mass of the central protostar derived from modeling the spectral energy distribution (SED) would be as high as 10–20  $M_{\odot}$ , and the temperature would be 4000–10 000 K, equivalent to a B2 star or earlier. Such a star should have detectable radio continuum and strong 24  $\mu\text{m}$  MIR emission, which contradicts observational evidence. On the other hand, the near-side distance of 5.7 kpc results in more reasonable physical parameters for JCMT18354–0649S.

Early explorations have mixed the emission and absorption spectra of G25.4NW with the nearby giant HII region W42 (Blum et al. 2000) due to low resolution. The methods of using the OH absorption features and scale height carry a large uncertainty. Anderson & Bania (2009) used the HI Emission/Absorption method with the high resolution HI survey data from the Very Large Array (VLA) Galactic Plane Survey (VGPS) and Southern Galactic Plane Survey (SGPS) to resolve the ambiguity in kinematic distance for a sample of HII regions from the inner Galaxy. In the catalog, they quoted a near-side distance of 5.9 kpc for G25.4NW. In this paper, we present the HI absorption feature associated with the UCHII region G25.4NW to confirm the result of the near-side distance, and give new estimates for the related physical parameters, such as the FIR luminosity and spectral type of the massive stars in G25.4NW. Using <sup>13</sup>CO (1–0) data from the Galactic Ring Survey, we also discuss the environment of the molecular cloud associated with the UCHII region.

## 2 DATA

The data sets for the radio continuum at 1420 MHz and HI emission were obtained from the VGPS, described in detail in Stil et al. (2006). The continuum images of G25.4NW shown in this paper have a spatial resolution of 1' at 1420 MHz and an rms sensitivity of 0.3 K ( $T_b/S_{\nu} = 168 \text{ K Jy}^{-1}$ ). The synthesized beam for the HI line images is also 1', and the radial velocity resolution is 1.56 km s<sup>-1</sup>. The short-spacing information for the HI spectral line images comes from additional observations performed with the 100 m Green Bank Telescope managed by NRAO.

The data sets from observations of the <sup>13</sup>CO-line ( $J = 1 - 0$ ) were collected from the Galactic Ring Survey (Jackson et al. 2006) carried out with the Five College Radio Astronomy Observatory's 14 m telescope. The CO-line data used in this paper have a velocity coverage of –5 to 135 km s<sup>-1</sup>, an angular resolution of 45'' with 22'' sampling, a radial velocity resolution of 0.21 km s<sup>-1</sup> and an rms noise of  $\sim 0.13 \text{ K}$ .

The *Spitzer* 8.0  $\mu\text{m}$  images are taken from the Galactic Legacy Infrared Mid-Plane Survey Extraordinaire (GLIMPSE; Benjamin et al. 2003) using the Infrared Array Camera (IRAC) (Fazio et al. 2004). The IRAC data were processed by the GLIMPSE team; image mosaics were created

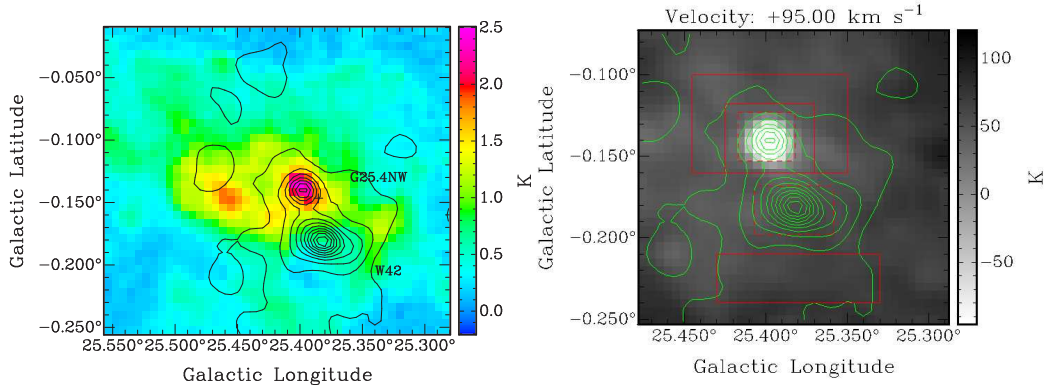


**Fig. 1** The VGPS 1420 MHz continuum contours of G25.4NW overlaid on (*left*) the  $^{13}\text{CO}$  integrated intensity image (over the range  $90\text{--}101\text{ km s}^{-1}$ ) and the HI single-channel map (*right*) at  $95\text{ km s}^{-1}$  for the GMC G25.4–0.14 region. Contours are overlaid which show the 1420 MHz continuum emission at the level of  $3\sigma$  ( $\sigma = 1\text{ K}$ ) above the background emission of  $29\text{ K}$ , and start from  $67\text{ K}$  in steps of  $57\text{ K}$ . The plus sign marks the position of the massive protostar JCMT18354–0649IRS1a found by Zhu et al. (2011).

using the GLIMPSE pipeline after artifacts such as cosmic rays, stray light, column pull-down and banding had been removed.

### 3 RESULTS AND ANALYSIS

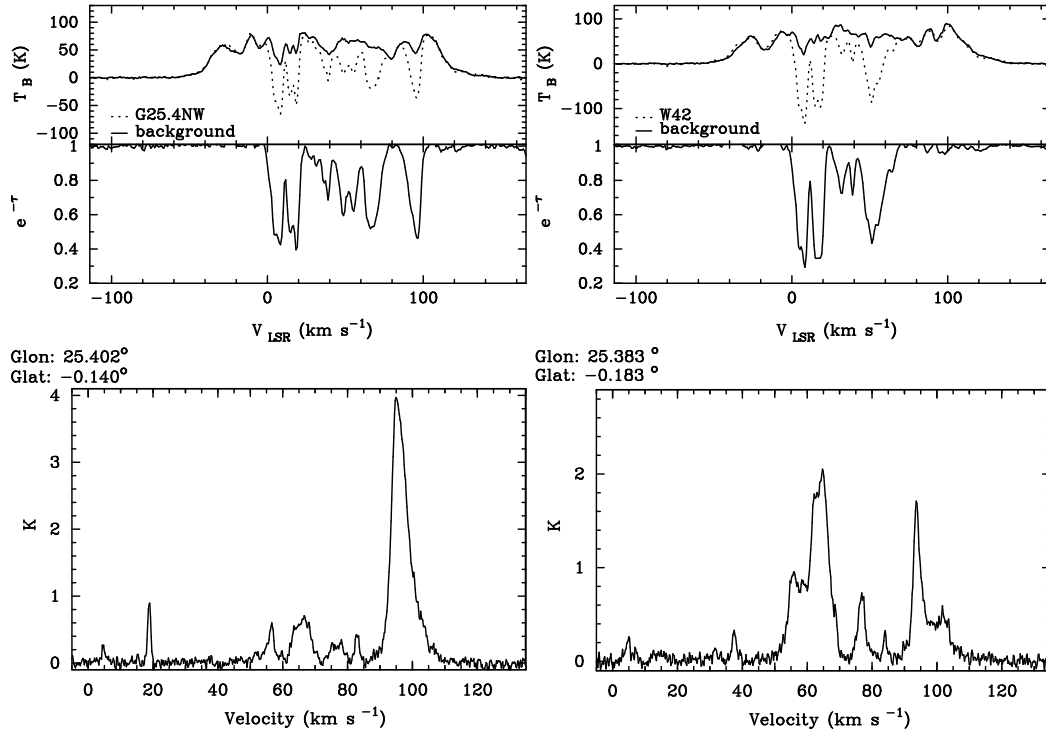
#### 3.1 Continuum Images

Figure 1 (left) shows the VGPS 1420 MHz continuum contours overlaid on the  $^{13}\text{CO}$  integrated intensity image (over the range  $90\text{--}101\text{ km s}^{-1}$ ) for the G25.4–0.14 region. Two radio sources, separated by about  $2'$ , are marked on the map, namely G25.4NW ( $l = 25.40^\circ$ ,  $b = -0.14^\circ$ ) and W42 ( $l = 25.38^\circ$ ,  $b = -0.18^\circ$ ). The later is also named G25.4SE in Lester et al. (1985). A massive protostar JCMT18354–0649IRS1a was recently discovered about  $1'$  south of G25.4NW (Zhu et al. 2011), which is marked as a plus sign. Contours of the 1420 MHz continuum emission starting from  $67\text{ K}$  in steps of  $57\text{ K}$  define a roughly circular region with a diameter of  $\sim 1.2'$ . As shown in Lester et al. (1985), G25.4NW has a size of about  $25''$  which is not resolved in this map.

#### 3.2 The HI Absorption Spectra and Kinematic Distance

We have searched the VGPS data with radial velocity ranging from  $-113$  to  $165\text{ km s}^{-1}$  for features in HI absorption which might be related to the morphology of G25.4NW. There are HI absorption features towards the direction of the HII region at the following velocities:  $5$ ,  $20$ ,  $40$ ,  $50$ ,  $55$ ,  $67$  and  $95\text{ km s}^{-1}$ . These HI absorption features towards the continuum intensity of G25.4NW are caused by absorption in HI clouds between the HII region and Earth. Figure 1 (right) shows the map of HI absorption at the channel with the highest absorption velocity of  $95\text{ km s}^{-1}$ . The map has superimposed contours of 1420 MHz continuum emission, which mark the HII regions.

We construct the HI emission and absorption spectra of G25.4NW in the same way as developed by Tian & Leahy (2008); Anderson & Bania (2009). To minimize the possible difference in the HI distribution along the two lines of sight (on-source and background), a background region is chosen



**Fig. 2** *Upper panels:* HI emission and absorption spectra extracted from the boxes around G25.4NW (left) and W42 (right) indicated in Fig. 1. *Lower panels:* Averaged <sup>13</sup>CO emission spectra of the G25.4NW (left) and W42 (right) region. The emission peak at 90–101 km s<sup>-1</sup> in the W42 <sup>13</sup>CO spectra comes from the G25.4NW molecular cloud due to the box selection.

near the continuum peak, as shown in Figure 1 (right). Assuming that the spin temperature and optical depth of the background region are similar to that of the on-source region, the resulting difference in brightness temperature at velocity  $v$  is given by  $\Delta T(v) = T_{\text{off}}(v) - T_{\text{on}}(v) = T_c(1 - e^{-\tau(v)})$ . Here  $T_{\text{on}}(v)$  and  $T_{\text{off}}(v)$  are the average HI brightness temperatures of the HII region and the adjacent background region from a selected area.  $T_c$  is the average continuum brightness temperature of the HII region.  $\tau(v)$  is the HI optical depth from the continuum source to the observer.

Figure 2 (upper left panel) shows the source and background HI emission, and the absorption spectra for the selected region on the top of G25.4NW. The  $T_{\text{on}}$  is obtained by averaging over the region outlined by a dashed-line box (Fig. 1 right). The respective off-source region is defined by the region between two solid-line boxes, within which the  $T_{\text{off}}$  is obtained. The averaged continuum temperature of G25.4NW is 154 K. Figure 2 clearly reveals strong absorption features at 5, 20, 40, 50, 55, 67 and 95 km s<sup>-1</sup>. The highest absorption velocity detected is close to the tangential velocity of 120 km s<sup>-1</sup>, but there are no absorption features between them, which indicates a near-side distance. Taking a circular Galactic rotation curve model, and using the latest estimates of the model parameters, i.e.  $V_0=220$  km s<sup>-1</sup> and  $R_0=8.5$  kpc (Fich et al. 1989), we can determine the kinematic distance using the distance-velocity curve as illustrated in Figure 3. The highest absorption velocity feature at 95 km s<sup>-1</sup> corresponds to a near-side distance of 5.7 kpc.

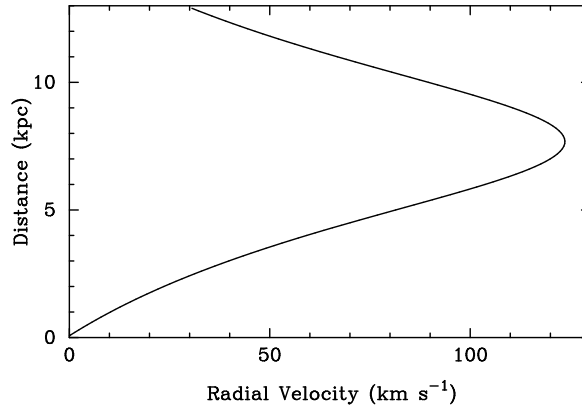


**Fig. 3** The relation between the distance and radial velocity for the assumed rotation curve.

**Table 1** Summary of HI and CO Velocity Features

Crossing number	Local	1	2	3	4	5	6
Central velocities of the model spiral arms ( $\text{km s}^{-1}$ )	0	26	71	93	52	21	0
G25.4NW HI absorption feature	0–10	10–20	60–80	90–100			
G25.4NW CO emission feature	5	15–20	75–85	90–100	50–60	15–20	5
W42 HI absorption feature	0–10	15–20	50–65				
W42 CO emission feature	5	32	60–70	90–100	50–60	15–20	5

For comparison, we also produce the HI absorption spectrum for the selected region of W42, as shown in the upper right panel of Figure 2. The averaged continuum temperature of W42 is 225 K. The highest HI absorption feature lies at 50–65  $\text{km s}^{-1}$ . It is far from the tangential velocity of 120  $\text{km s}^{-1}$ , and also indicates a near-side distance of 4.6 kpc. The emission peak at 90–101  $\text{km s}^{-1}$  in the W42  $^{13}\text{CO}$  spectra comes from the G25.4NW molecular cloud due to the place where the box was selected in the right panel of Figure 1. Higher resolution observations will improve the localization of these values.

The optically thin  $^{13}\text{CO}$  emission could clearly reveal the distribution of molecular clouds along the direction of the HII region, and will indicate a possible origin of these HI absorption features.

Figure 2 (lower left panel) shows an average  $^{13}\text{CO}$  spectrum for the full velocity range in the direction of G25.4NW. It shows seven molecular components with high brightness temperature, at radial velocities of 5, 18, 55, 65, 78, 83 and 95  $\text{km s}^{-1}$  respectively. Most of the  $^{13}\text{CO}$  emission peaks appear to be associated with an HI absorption feature, and the  $^{13}\text{CO}$  emission velocities are consistent with radial velocities of the spiral arm in the Milky Way based on the Galactic arm model (Cordes & Lazio 2002).

In Table 1 we list the respective spiral arm radial velocities and possible associations with  $^{13}\text{CO}$  emission or HI absorption features. Cases are included even when the velocities have differences up to  $\sim 10 \text{ km s}^{-1}$ , since the crossing velocities of the calculated arm are based on a circular rotation model and can be off by  $\sim 10 \text{ km s}^{-1}$  due to non-circular motions from spiral arm shocks and velocity dispersion.

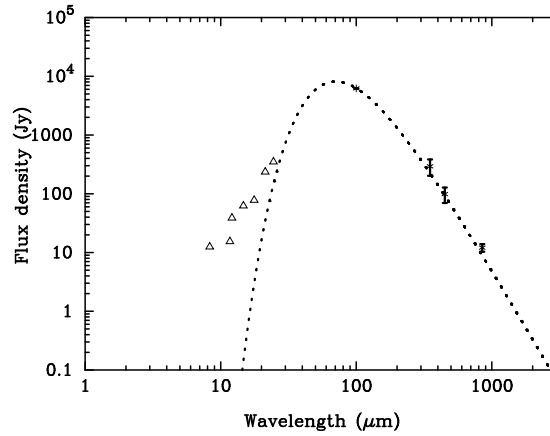


**Fig. 4** Flux density distribution of G25.4NW fitted with a one-component modified black-body model. The line marks the best fit to the 100, 350, 450 and 850  $\mu\text{m}$  flux densities with  $T_d=41.2\pm 2.8$  K.

**Table 2** Summary of Observed Flux Densities of G25.4NW

Wavelength ( $\mu\text{m}$ )	Flux (Jy)	Error (Jy)	Aperture ( $''$ )
8.3	12.51	–	18.3
12.1	38.86	–	18.3
14.7	62.48	–	18.3
21.3	235.88	–	18.3
11.7	15.4	0.5	10.8
17.7	78.0	3	10.8
24.5	350.0	80	10.8
100	6240.0	–	50
350	293.0	91	50
450	98.7	29	50
850	12.1	1.8	50

In summary, both W42 and G25.40–0.14 are at the near side distance, and they appear to be located in the inner galactic CO ring at 4–6 kpc.

## 4 DISCUSSION

### 4.1 Infrared Emission

Dust associated with HII regions can absorb radiation from the exciting stars in nebulae and re-emit in infrared wavelengths. If there is sufficient spatial coverage and optical depth of dust surrounding an HII region, measurement of the infrared flux from the HII region can provide information on the bolometric luminosity ( $L_{\text{bol}}$ ) of the exciting stars.

We collect the total MIR flux densities of the IR counterparts for G24.5NW in the literature (Table 2), including data from the *MSX* point-source catalog (8.3, 12.1, 14.7 and 21.3  $\mu\text{m}$ ), Keck I 10 m telescope (11.7, 17.65, 24.5  $\mu\text{m}$ ) (Giveon et al. 2007), *IRAS* 100  $\mu\text{m}$  (Lester et al. 1985), *CSO* (350  $\mu\text{m}$ ) and *SCUBA* (450  $\mu\text{m}$ , 850  $\mu\text{m}$ ) (Wu et al. 2005). *MSX* had a beam of 18.3 $''$ , and

the Keck data had an aperture of  $10.5''$ . The  $100\ \mu\text{m}$  beam is  $50''$ , which is much larger than that of the CSO and SCUBA data. We used an aperture of  $50''$  to derive the sub-millimeter fluxes in order to cover the whole HII region. The dust emissivity index ( $\beta$ ) has been estimated to be a typical value of 2.0 (Zhu et al. 2011). Thus we used a modified single temperature blackbody curve,  $\nu^2 B_\nu(T_d)$ , to fit the data and derive the SED. In lieu of a radiative transfer model, we have chosen to fit the cold component of the emission ( $100\text{--}850\ \mu\text{m}$ ) because it contains the bulk of the source luminosity. The SED fitting is plotted in Figure 4. The best fit parameter is  $T_d=41.2\pm 2.8\ \text{K}$ . It is larger than that estimated in Zhu et al. (2011), considering the contribution of MIR data in the SED fitting, which traces the central bright temperature component.

For a distance of 5.7 kpc we obtain  $\log(L_{\text{bol}}/L_\odot)=5.6$ . This value is lower than the result of Churchwell et al. (1990) which was estimated from the far-IR data using a far-side distance. Thus the central stars are not as hot as previously estimated, and an O6 star is expected for such bolometric luminosity (Panagia 1973).

#### 4.2 Radio Emission

Radio continuum measurements of HII regions can provide a lower limit to the total number of ionizing photons ( $N_L$ ) and estimates of the average excitation parameter ( $U$ ). Assuming an optically thin, spherical, HII region with constant density, the equations used are as follows (Rudolph et al. 1996),

$$N_L = 7.5 \times 10^{43} S_\nu d^2 \nu^{0.1} T_e^{-0.45} [\text{s}^{-1}], \quad (1)$$

$$U = 1.33 S_\nu^{1/3} d^{2/3} \nu^{1/30} T_e^{0.116} [\text{pc cm}^{-2}], \quad (2)$$

where  $\nu$  is the frequency in GHz,  $S_\nu$  is the flux density measured at frequency  $\nu$  in mJy,  $d$  is the distance to the source in kpc and  $T_e$  is the electron temperature in units of  $10^4\ \text{K}$ . Parameter values used are  $\nu=1.42\ \text{GHz}$ ,  $d = 5.7\ \text{kpc}$  and  $T_e = 10000\ \text{K}$ . A general value of  $10^4\ \text{K}$  is used because the results of both  $N_L$  and  $U$  are not sensitive to  $T_e$ ,

The flux density for G25.4NW obtained from the VGPS continuum image is  $1.35\pm 0.2\ \text{Jy}$ , which is in agreement with Giveon et al. (2007) from a 1.4 GHz survey using the VLA in B configuration with a resolution of  $\sim 5''$ . This yields values of  $N_L = (3.4 \pm 0.2) \times 10^{48}\ \text{s}^{-1}$  and  $U = 47.5 \pm 10\ \text{pc cm}^{-2}$ . Comparing these values ( $\log N_L=48.5$ ) to those of Panagia (1973), we estimate an ionizing flux and excitation parameters corresponding to an O6–O7 class star. From the 3-color HKL' band image (fig. 3 in Zhu et al. 2011), it is more likely that the ionizing flux comes from several stars. It is possible that G25.4NW is powered by several O/B stars, with at least one earlier than an O7 star.

#### 4.3 Ionized Gas Mass

For optically thin emission, the emission measure (EM) is related to the surface brightness ( $I_\nu$ ) according to the following formula (Osterbrock 1989)

$$I_\nu = 2\nu^2 k T_{b\nu} / c^2 = j_\nu \int n_i n_e ds = j_\nu \text{EM}, \quad (3)$$

where  $j_\nu$  is the free-free emissivity for  $\text{H}^+$  ( $3.45 \times 10^{-40}\ \text{erg cm}^{-3}\ \text{s}^{-1}\ \text{Hz}^{-1}\ \text{sr}^{-1}$  at 1420 MHz and 7500 K; after Lang 1980),  $n_i$  is the ion density and  $n_e$  is the electron density. For  $j_\nu$  of a pure hydrogen nebula one can write

$$\text{EM} = 5.77 \times 10^2 T_{b\nu} \left( \frac{T_e}{7500\ \text{K}} \right)^{0.35} \left( \frac{\nu}{1.42\ \text{GHz}} \right)^{2.1} [\text{cm}^{-6}\ \text{pc}], \quad (4)$$



$$T_{b\nu} = \frac{c^2 S_\nu 10^{-26}}{2k\nu^2 \Omega} [\text{K}], \quad (5)$$

where  $T_e$  is the electron temperature in the nebula,  $S_\nu$  is the integrated flux density in Jy and  $\Omega$  is the radio source solid angle in steradians. The UCHII region was not resolved in the VGPS map (resolution  $1'$ ), but it is resolved in the high resolution map observed with the VLA in B configuration (Giveon et al. 2005), from which we estimated that the source has a size of  $10.1''$ , corresponding to a physical size of  $\sim 0.28$  pc. Hence we derive  $\text{EM} = 5.5 \times 10^6 \text{ cm}^{-6}$  pc using a typical value of  $T_e = 10000$  K. The electron density in the HII region can be calculated from the emission measures using the following formula (Giveon et al. 2007)

$$n_e = 990 \sqrt{\left(\frac{\text{EM}}{10^6 \text{ pc cm}^{-6}}\right) \left(\frac{\text{pc}}{D}\right)} [\text{cm}^{-3}] \quad (6)$$

where  $D$  is the diameter of G25.4NW ( $\sim 0.28$  pc). We find an average value of  $n_e = 4.4 \times 10^3 \text{ cm}^{-3}$ . Assuming a spherical volume of ionized gas, we estimate that G25.4NW contains  $460 M_\odot$  of ionized gas.

Comparing the EM and  $n_e$  values with those in Giveon et al. (2007) (after correcting the distance from 9.6 to 5.7 kpc), our derived values are slightly lower than theirs. This is because we used a larger source size. Giveon et al. (2005) used the 5 GHz VLA data to estimate a source size of  $3.7''$ , thus they obtained values for a more compact HII region. As the NIR map of Zhu et al. (2011) has shown there are at least three stars in the G25.4NW region; the VLA map at 1.4 GHz could not resolve the individual HII region, thus we could be overestimating the source size. Nevertheless, our estimated values of EM and  $n_e$  can be used as a lower limit.

#### 4.4 The Giant Molecular Cloud Surrounding G25.4NW

Figure 5 shows the  $^{13}\text{CO}$  integrated intensity contours (over the range  $90\text{--}101 \text{ km s}^{-1}$ ) overlaid on the IRAC  $8 \mu\text{m}$  image. The MIR  $8 \mu\text{m}$  emission is dominated by the PAH emissions that are heated by UV photons from young stars. The two bright regions in the map are the HII regions G25.4NW and W42. The W42 region is not physically related to G25.4NW. It is a foreground source at a different distance of 4.6 kpc (see Sect. 3.2). We can see that G25.4NW is embedded in a giant molecular complex, which appears to be divided into two major clouds: the fish-shaped cloud G25.40–0.14 hosting G25.4NW and the other one, G25.65–0.10, that peaks at  $(l = 25.68^\circ, b = -0.13^\circ)$ . The latter was named G25.65–0.10 in the paper of Solomon et al. (1987), which appears to be associated with an IR dark cloud. We note that Solomon et al. (1987) use G25.65–0.10 to refer to the GMC at  $94 \text{ km s}^{-1}$ , with a size of  $13' \times 8'$ , which did not include the G25.4–0.14 cloud. However, in our maps these two clouds appear to be associated with each other, connected by low level contours (as shown in the  $3\sigma$  contour), indicating a possible physical connection between G25.4–0.14 and G25.65–0.10; they might belong to one GMC at the same distance. If confirmed, such a GMC would have a maximum physical size of about 36 pc ( $22'$ ) at a distance of 5.7 kpc. The two separate major clouds and the existence of a number of local peaks in each cloud suggest that fragmentation is taking place in this complex, with G25.4NW being the most active region forming a cluster of massive stars. JCMT18354–0649S, as another massive core that hosts a massive protostar, is offset from the G25.4NW radio continuum by  $1'$ , indicating that OB stars leave their natal clouds and the HII region is more evolved. It appears that the massive stars that formed are triggering new star formation in JCMT18354–0649S. We have searched the literature and the SIMBA database, and there are no IR or radio sources associated with G25.65–0.10, suggesting that this cloud is relatively quiet and no star forming activity is taking place.

The total mass of  $\text{H}_2$  in the fish-shaped CO cloud G25.4–0.14 (size:  $12' \times 6'$ ) at  $95 \pm 10 \text{ km s}^{-1}$  is estimated using  $M_{\text{H}_2} = N_{\text{H}_2} \Omega d^2 (2m_{\text{H}}/M_\odot)$ , where  $\Omega$  is the solid angle of the cloud, and  $d$



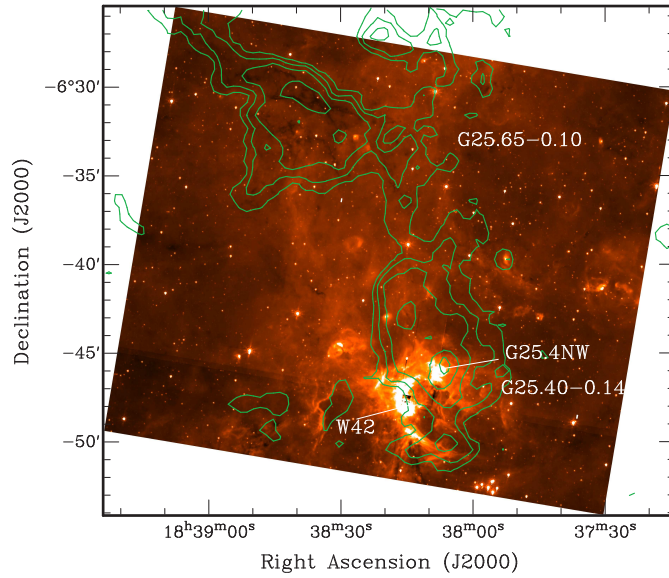


**Fig. 5** The  $^{13}\text{CO}$  integrated intensity contours overlaid on a *Spitzer* IRAC 8  $\mu\text{m}$  image. The contours are plotted at 0.6 ( $3\sigma$ ), 0.8, 1.1, 1.6 and 2.2 K.

is its distance of 5.7 kpc. Assuming the CO cloud is under thermodynamic equilibrium and the  $^{13}\text{CO}$  is optically thin and using the fitted dust temperature of 42.5 K, we obtained a  $^{13}\text{CO}$  column density of the cloud of  $N_{^{13}\text{CO}} = 2.91 \times 10^{17} \text{ cm}^{-2}$  from the  $^{13}\text{CO}$  integrated map (over the range 90–101  $\text{km s}^{-1}$ ). Then we obtain an average  $\text{H}_2$  column density of  $N_{\text{H}_2} = 4.59 \times 10^5 N_{^{13}\text{CO}} \approx 1.33 \times 10^{23} \text{ cm}^{-2}$ , and a molecular cloud mass of  $M_{\text{H}_2} \approx 1.0 \times 10^4 M_{\odot}$ . This molecular cloud has a mean density of  $\sim 2.3 \times 10^4 \text{ cm}^{-3}$ .

## 5 SUMMARY

In summary, using the new VLA continuum and HI-line data for G25.4NW, we have obtained HI absorption profiles towards the UCHII region. G25.4NW shows HI absorption features up to 95  $\text{km s}^{-1}$ , and there are no other absorptions up to the tangential velocity, giving a near-side distance of 5.7 kpc. The detected HI absorption and CO emission are coincident with the expected velocity for a region hosting the galactic molecular ring at 4–6 kpc, as derived from the model of the Galactic arms. Using the new distance, we obtain a bolometric luminosity of  $10^{5.6} L_{\odot}$  with IR emission collected from G25.4NW, which corresponds to an O6 star. We also use the radio continuum emission data to confirm this result, and re-calculate the EM and electronic density  $n_e$ . We estimate that G25.4NW contains 460  $M_{\odot}$  of ionized gas. The  $^{13}\text{CO}$  data reveal that G25.4NW is part of a more extended star forming complex with about  $10^4 M_{\odot}$  of molecular gas.

**Acknowledgements** We acknowledge the support from the National Natural Science Foundation of China (Grant No. 11073028), the National Basic Research Program of China (973 program, 2012CB821800), the Young Researcher Grant of NAOC and also from the “Hundred-talent program” of the Chinese Academy of Sciences. We thank Prof. Wenwu Tian, Yuefang Wu and Dr. Lei Zhu for reviewing the manuscript and providing helpful instruction. We thank the anonymous referee for his or her instructive and useful comments.

## References

- Anderson, L. D., & Bania, T. M. 2009, *ApJ*, 690, 706
- Benjamin, R. A., Churchwell, E., Babler, B. L., et al. 2003, *PASP*, 115, 953
- Blum, R. D., Conti, P. S., & Daminieli, A. 2000, *AJ*, 119, 1860
- Carolán, P. B., Khanzadyan, T., Redman, M. P., et al. 2009, *MNRAS*, 400, 78
- Churchwell, E., Walmsley, C. M., & Cesaroni, R. 1990, *A&AS*, 83, 119
- Cordes, J. M., & Lazio, T. J. W. 2002, arXiv:astro-ph/0207156
- Downes, D., Wilson, T. L., Bieging, J., & Wink, J. 1980, *A&AS*, 40, 379
- Fazio, G. G., Hora, J. L., Allen, L. E., et al. 2004, *ApJS*, 154, 10
- Fich, M., Blitz, L., & Stark, A. A. 1989, *ApJ*, 342, 272
- Giveon, U., Becker, R. H., Helfand, D. J., & White, R. L. 2005, *AJ*, 129, 348
- Giveon, U., Richter, M. J., Becker, R. H., & White, R. L. 2007, *AJ*, 133, 639
- Jackson, J. M., Rathborne, J. M., Shah, R. Y., et al. 2006, *ApJS*, 163, 145
- Lester, D. F., Dinerstein, H. L., Werner, M. W., et al. 1985, *ApJ*, 296, 565
- Liu, T., Wu, Y., Zhang, Q., et al. 2011, *ApJ*, 728, 91
- Osterbrock, D. E. 1989, *S&T*, 78, 491
- Panagia, N. 1973, *AJ*, 78, 929
- Rudolph, A. L., Brand, J., de Geus, E. J., & Wouterloot, J. G. A. 1996, *ApJ*, 458, 653
- Solomon, P. M., Rivolo, A. R., Barrett, J., & Yahil, A. 1987, *ApJ*, 319, 730
- Stil, J. M., Taylor, A. R., Dickey, J. M., et al. 2006, *AJ*, 132, 1158
- Tian, W. W., & Leahy, D. A. 2008, *ApJ*, 677, 292
- Turner, B. E. 1979, *A&AS*, 37, 1
- Wu, Y., Zhu, M., Wei, Y., et al. 2005, *ApJ*, 628, L57
- Zhu, M., Davis, C. J., Wu, Y., et al. 2011, *ApJ*, 739, 53